Journal of Marine Research, 67, 385–409, 2009

Journal of
MARINE RESEARCH

Volume 67, Number 4

A linear diffusivity model of near-surface, cross-shore particle dispersion from a numerical simulation of central California's coastal ocean

by Patrick T. Drake[1,2] and Christopher A. Edwards[1]

ABSTRACT

A simple diffusion model of cross-shore mixing employing an inhomogeneous diffusivity is applied to near-surface particle dispersion within a high-resolution numerical model of the central California coastal ocean. The theoretical model employs a linear diffusivity, $K_y = \nu y$, where y is the cross-shore coordinate and ν a constant, as traditionally assumed for wall-layer flows. A realistic implementation of the Regional Ocean Modeling System (ROMS) is used to generate hundreds of thousands of three-dimensional, passive particle trajectories. Particles were released daily along the inner shelf for one model year, 2002, tracked for 16 days and treated statistically as an instantaneous point-source release. Application of the theoretical model to the observed moments of particle position yielded estimates for the offshore slope of the diffusivity, $\nu \sim 3 - 4$ cm s^{-1}. Using this value, the cross-shore particle density was well described over the outer continental shelf and slope by an analytical solution to the theoretical model. Unlike wall turbulence, the implied mixing length was not equal to the distance from the coast, but was found to be equal to the local first mode internal Rossby radius of deformation. The successful theoretical model has many potential applications, such as quantifying the amount of offshore larval loss from the shelf and/or carbon loss from the coastal upwelling zone.

1. Introduction

The dispersion of passive particles by ocean circulation is a complex phenomena encompassing many diverse processes, all interacting over a wide range of time and space scales (Okubu, 1971; Davis, 1991a). Its accurate prediction can be especially challenging in the

1. Ocean Sciences Department, University of California Santa Cruz, Santa Cruz, California, 95064, U.S.A.
2. Corresponding author. ***email: pdrake@ucsc.edu***

coastal ocean, where relatively small-scale inhomogeneities in the bathymetry and circulation complicate the application of idealized theories (Largier, 2003). Despite this complexity, a variety of environmental disciplines need practical answers to seemingly simple dispersion questions, such as: How far will the particles of interest be transported in a given time? or What fraction will remain in the local water column?

Oceanographers typically view dispersion as a combination of advection and diffusion. This approach reduces the ocean's natural complexity down to two specific scales: the mean flow, representing the lowest-frequency and largest scales of motion, and the turbulence, representing any higher-frequency or smaller-scale variability the mean flow fails to resolve (Swenson and Niiler, 1996). In this view, dispersing particles constitute a passive tracer cloud that is both advected by the mean flow and diffused by unresolved turbulent eddies. The diffusive flux of tracer is often parameterized using a Fickian flux-gradient law and an Eulerian eddy diffusivity, K, which characterizes all of the unresolved motion (Swenson and Niiler, 1996; Boning and Cox, 1988; Taylor, 1921). Generally assumed to vary slowly in time and space, K is a critical parameter for studies of coastal dispersion (Largier, 2003). When the turbulence is homogeneous and stationary, K can be determined directly from Lagrangian particle statistics (Bauer *et al.*, 1998; Swenson and Niiler, 1996). However, given the general inhomogeneity and non-stationarity of the ocean, the method that best estimates K remains an open question (Zhurbas and Oh, 2003; Bauer *et al.*, 1998; Swenson and Niiler, 1996).

In this study, we investigate how well a simple diffusion model employing a linear Eulerian diffusivity can predict cross-shore, near-surface particle dispersion simulated by a state-of-the-art coastal ocean circulation model. A linear cross-shore diffusivity, zero at the coast and growing offshore, has been used successfully by previous authors to explain (a) the moments of particle position for surface drifters launched off the central California shelf (Davis, 1985) and (b) exit-time statistics for subsurface (275–375 m) drifters launched off the central California slope (Ivanov *et al.*, 2008, 2009). Employing a vastly increased number of floats than these previous studies, we follow the method of Davis (1985) and determine the cross-shore diffusivity, K_y, from the time-behavior of the particle moments. We extend this method significantly by comparing the float density to an analytical solution to the theoretical diffusion model, allowing for a successful test of both the linear diffusivity assumption and the specific value of K_y. Although the theoretical model neglects advection and clearly omits many of the complexities of dispersion in the real coastal ocean, aspects of this simple model are surprisingly robust when averaged over a large ensemble of particle release dates, release locations and oceanic flow conditions. Alongshore measurements of particle position are presented to give some general context, but the study focuses on the cross-shore dimension because a simple, testable theory exists in this case. The simple yet successful theory allows for a better understanding of offshore particle flux and has many potential practical applications, such as quantifying the amount of larval loss from the shelf and/or carbon export from the coastal upwelling zone.

A realistic, high-resolution numerical model of the coastal circulation off central California is employed to obtain particle trajectories. The numerical model reproduces many

features observed in the real ocean and accurately predicts observed turbulent velocity scales. Into the simulated currents we release hundreds of thousands of passive point particles, or floats. They are introduced daily for nearly one model year at a variety of depths over the inner shelf, the most relevant release location for many tracers of practical interest such as pollutants and larvae. Particle trajectories are tracked for 16 days and reprocessed to mimic an instantaneous, point-source release, a case for which substantial theory has been developed (Csanady, 1973). We compare the simple diffusion model to the observed statistics and infer values for K_y. Using this measured diffusivity, we then compare the observed particle density to an analytical solution predicted by the theory. Lastly, we show that the cross-shore mixing-length implied by the diffusivity is equal to the first mode internal Rossby radius of deformation.

2. Numerical model description and evaluation

The Regional Ocean Modeling System (ROMS) is employed to simulate the circulation of the central California ocean. Its core is a hydrostatic, primitive equation numerical model with a free surface (Shchepetkin and McWilliams, 2005). The model is computationally efficient as a result of time-splitting of barotropic and baroclinic components, and includes a wide range of subgridscale parameterizations for vertical mixing. Discretized in curvilinear coordinates and along sigma, terrain-following coordinates, the code is ideally suited to coastal problems and has been widely applied in such settings.

The present implementation of ROMS consists of a three-way nested configuration (Fig. 1). All ocean domains are driven at the surface by fields provided by the Coupled Ocean Atmosphere Mesoscale Prediction System (COAMPS), a quadruply nested non-hydrostatic, data assimilative model of the northeast Pacific region (Hodur, 1997; Hodur *et al.*, 2002). Hourly COAMPS fields were first daily averaged before input into the model. The outermost ROMS nest exists at 1/10 degree resolution, and lateral boundary fields are obtained from a 1-degree, monthly product from the ECCO project. ECCO, from Estimating the Circulation and Climate of the Ocean, consists of a family of global ocean data assimilative state estimates (Heimbach *et al.*, 2006; 2008; Wunsch *et al.*, 2007). The model contains neither tides nor a sea breeze.

The outermost grid has a configuration similar to that described and evaluated in Veneziani *et al.* (2009), the main difference being the 39-degree rotation of the present grid(s) relative to longitude and latitude. The middle nest exists at 1/30 degree resolution, and lateral boundary conditions to this domain are provided by the outermost model output. Similarly, the 1/90 degree innermost domain is influenced at the lateral boundaries by the modeled fields from the middle grid. This nested configuration results in a high-resolution inner domain centered over the central California coastal ocean. The wet extent of the inner domain is $\sim$400 km alongshore and $\sim$200 km cross-shore, with a nearly isotropic horizontal grid spacing of 1.1–1.2 km. The inner model consists of 42 vertical levels and utilizes a KPP (Large *et al.*, 1994) parameterization of subgridscale vertical mixing. All model fields and

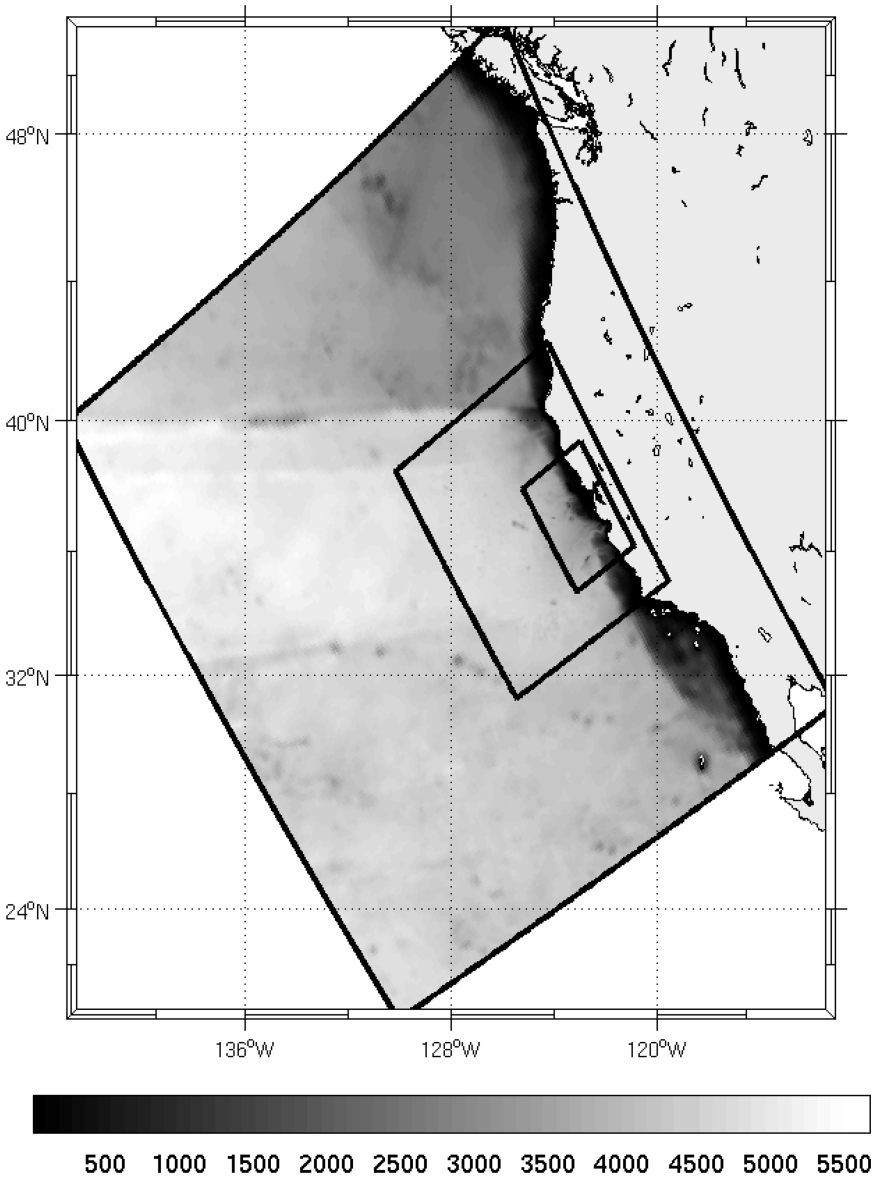

Figure 1. North American west coast with nested model grids. Gray-scale map shows water depth (m).

Eulerian and Lagrangian statistics presented below refer to this innermost high-resolution domain.

A horizontal snapshot of the model's temperature and velocity fields (Fig. 2) demonstrates that the model can reproduce many of the circulation features frequently observed in central California's coastal ocean. The depth shown is 20 m, close to the time-average float depth

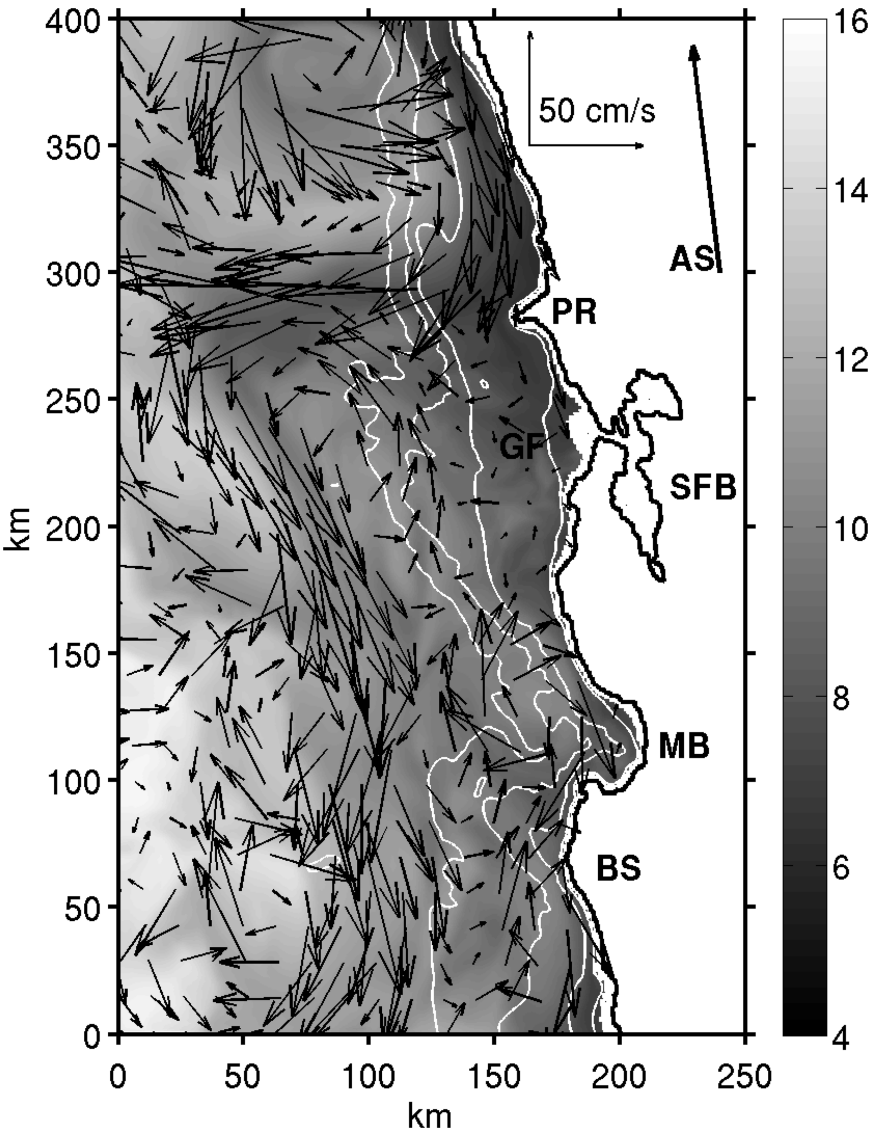

Figure 2. Simulated temperature (gray-scale map, in °C) and velocity (arrows) at 20 m depth on June 22, 2002, on a Cartesian representation of the innermost grid. Fine white lines are the 40, 200, 1000 and 2000 m isobaths. Bold arrow shows alongshore (AS) direction used in the float analysis. PR: Point Reyes. GF: Gulf of the Farallones. SFB: San Francisco Bay. MB: Monterey Bay. BS: Big Sur.

of 17 m (see Float processing below), and the date, June 22, 2002, is representative of spring upwelling conditions. A meandering, diffuse temperature front is visible roughly 100 km offshore of the coast, running in the alongshore direction throughout the entire domain.

This front separates cold, recently upwelled water from warmer offshore water and is one of the most prominent features of the California Current in spring (Kosro *et al.*, 1991). The front is associated with a southward flowing, meandering core current with strong instantaneous velocities of $\sim$50 cm s^{-1}. In the northern part of the domain, this current is found as an upwelling jet over the continental shelf north of Point Reyes, a feature that is well documented in the real ocean (Roughan *et al.*, 2006; Winant *et al.*, 1987). At Point Reyes, the jet connects with a cold filament oriented directly offshore, a phenomena also frequently seen in satellite images (Kosro *et al.*, 1991; Strub *et al.*, 1991). A large, well-organized eddy is visible just offshore of the jet in the far northern part of the domain. This location is close to Point Arena, which is known to be an area of strong eddy activity. Lastly, a smaller, anti-cyclonic eddy is also visible in the southern portion of the domain, just outside the mouth of Monterey Bay. A warm-core feature of this type has also been documented (Rosenfeld *et al.*, 1994).

An annual time average of the flow at 20-m depth is shown in Figure 3. The Eulerian rms eddy speed, defined as the square root of twice the mean Eulerian Eddy Kinetic Energy, or $(2\overline{EKE})^{1/2}$, is shown as a gray-scale map. In addition, the Eulerian time-average velocity vectors are overlain as arrows. Both statistics cover the period Jan. 6, 2002 – Jan. 1, 2003. The mean Eulerian Eddy Kinetic Energy, $\overline{EKE}$, was calculated as $0.5(\overline{u'^2 + v'^2})$, where the overbar represents a time average, the primed variables represent time fluctuations relative to the mean and (u, v) are the (alongshore, cross-shore) velocities, respectively. We prefer the statistic $(2\overline{EKE})^{1/2}$ because it represents the average magnitude of the velocity fluctuations and is directly comparable to velocity scales in cm s^{-1}. The Eulerian rms eddy speed is greatest in the northern part of the domain and smallest in Monterey Bay and the Gulf of the Farallones, two relatively sheltered environments. We note also the general spatial inhomogeneity of this statistic and the mean velocities. While there is an obvious pattern of southward flow over the domain as a whole, there are coherent pockets of northward motion, specifically offshore of the mouth of Monterey Bay and within the Gulf of the Farallones. A very-nearshore, northward flowing counter-current is also found over the inner shelf north of Point Reyes.

We compare model temperatures and velocities with observations from three moorings in the Monterey Bay area: SHB1, an inner-shelf mooring at a water depth of 20 m maintained by the Partnership for Interdisciplinary Studies of Coastal Oceans (PISCO), and M1 and M2, two Monterey Canyon moorings maintained by the Monterey Bay Aquarium Research Institute (MBARI) with water depths of 1600 m and 1800 m, respectively. (Moorings are heavy dots in Fig. 3). We note that many oceanographic features may be reproduced well by the model but displaced slightly in space or time, leading to potentially large errors in point-to-point mooring comparisons.

The comparisons were made at the nearest model gridpoint to the moorings. Daily-averaged temperatures and ADCP velocities from the moorings were compared with daily averages from the model for nine months at SHB1 (the longest period of continuous data, Jan. 15, 2002 – Oct. 15, 2002) and for 11 months at M1 and M2 (Jan. 15, 2002 – Dec. 15, 2002). Modeled temperatures were interpolated vertically between sigma levels to match

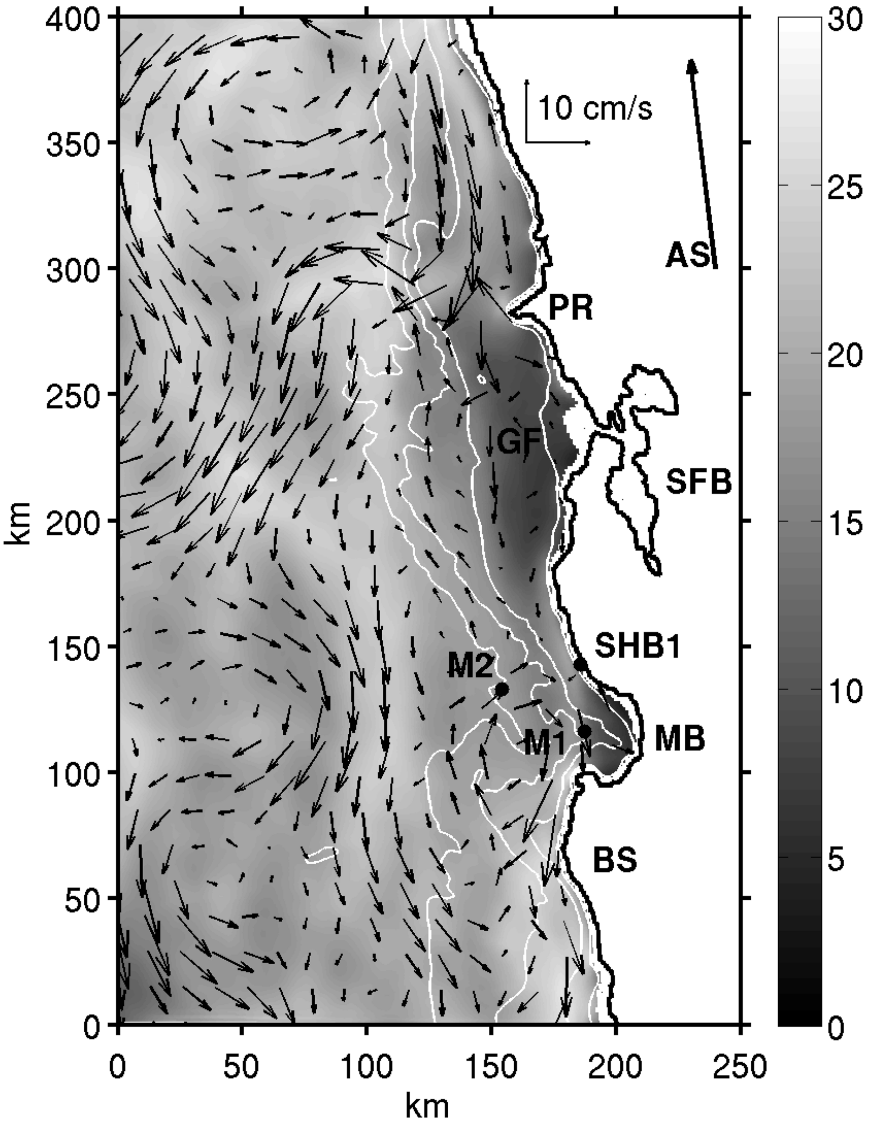

Figure 3. The Eulerian rms eddy speed $((2\overline{EKE})^{1/2}$ as gray-scale map) and time-mean velocities (arrows) at 20-m depth on a Cartesian representation of the innermost grid. Averaging period is Jan. 6, 2002 – Jan. 1, 2003. Heavy black dots are mooring locations: SHB1, M1 and M2. Fine white lines are the 40, 200, 1000 and 2000 m isobaths. Bold arrow shows alongshore (AS) direction used in the float analysis. PR: Point Reyes. GF: Gulf of the Farallones. SFB: San Francisco Bay. MB: Monterey Bay. BS: Big Sur.

Table 1. Near-surface observed (*obs*) and modeled (*mod*) temperature statistics, in °C. Zero-lag correlation(s), r, are significant to the 99 percent confidence level, with the exception of the M2 20-m depth, which is not significant. The 2002 comparisons covered 9 months at SHB1 and 11 months at M1 and M2.

station	mean_{obs}	mean_{mod}	std_{obs}	std_{mod}	r
SHB1 4 m	11.8	11.0	1.1	1.8	0.71
SHB1 12 m	11.2	10.6	0.9	1.7	0.86
M1 1 m	12.5	12.4	1.3	1.9	0.84
M1 20 m	11.5	11.3	0.9	1.6	0.82
M2 1 m	12.9	13.5	1.2	1.9	0.68
M2 20 m	12.1	12.2	0.9	1.5	N/S †

† Not significant.

the instrument depths. Comparison depths were chosen to be representative of the depths experienced by the floats. Velocities were averaged over the entire water depth at SHB1, where the flow is predominantly alongshore and typically lacks a zero-crossing in the vertical (Drake *et al.*, 2005). At M1 and M2, both a near-surface equatorward flow and poleward undercurrent may be present simultaneously. Thus we averaged over the depth range 12–28 m, corresponding to the top two ADCP depth-bins at these moorings, to capture the near-surface flow experienced by most of the floats.

The agreement between measured and simulated temperatures is good (Table 1). The mean values differ by 0.2–0.6 °C. The zero-lagged correlations between modeled and measured temperatures are also high and statistically significant to the 99 percent confidence level, with the exception of the 20 m depth at the deepest-water mooring, M2. (Confidence levels were estimated using an N^*, or degrees of freedom, found by dividing the total record length by the shortest decorrelation time-scale of either time series. A linear trend was removed from all time series before calculating correlations.) However, the model overestimates the size of the temperature fluctuations by about 60–70 percent. The temperature agreement is best at the inshore canyon mooring, M1, at a depth of 1 m, shown in Figure 4, top panel. The observed seasonal trend is clearly present in the model. The simulation also reproduces most of the weather-band or semi-weekly fluctuations, although it overestimates their size.

In general, the agreement between modeled and observed vector velocities at all three moorings is less compelling. For analysis, the currents are resolved into their respective principal axes. Major axes are oriented roughly alongshore at all sites (Table 2). At all three moorings mean flows are small ($\leq$6 cm s^{-1}) in both the model and observations, but not similarly directed. Modeled and observed velocity fluctuations are not well correlated. The agreement is best at M1, where the complex correlation coefficient (Kundu, 1976) is low, $\rho = 0.25$, but significant to the 99 percent confidence limit, with an average phase of 12 degrees. (Here, only the major-axis velocity is used to determine N^*) In Figure 4, bottom panel, we compare the major principal axis velocity anomaly at M1. The scales of variability are clearly similar between the observations and model. Instantaneous vertical

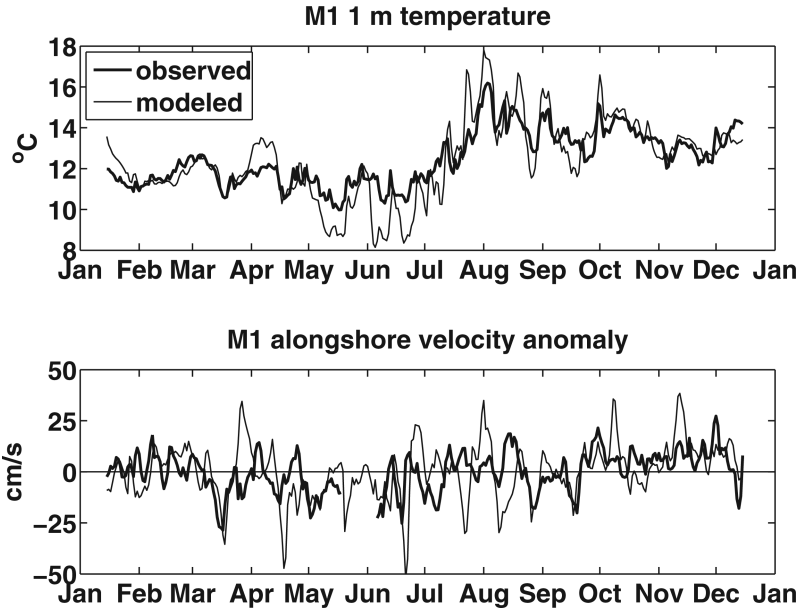

Figure 4. Point-to-point model-data comparison at M1 mooring. Top panel: temperature at 1 m depth. Bottom panel: major principal axis velocity anomaly, depth averaged over 12–28 m. Major axes were oriented approximately alongshore, or NNW (349°T for the observations and 333°T for the model).

shear in the observed horizontal velocities also displayed similar temporal variability in the model (not shown). At M1, observed values of the near-surface alongshore shear, $|\partial u/\partial z|$, varied from $\sim 1-7 \times 10^{-3}$ s^{-1}, with typical values near $\sim 2 \times 10^{-3}$. Modeled values were

Table 2. Near-surface observed (*obs*) and modeled (*mod*) Eulerian current statistics, in cm s^{-1}. The 2002 comparisons covered 9 months at SHB1 and 11 months at M1 and M2. Velocities were depth-averaged over 0–20 m at SHB1, and 12–28 m at M1 and M2. Currents were resolved into their principal axes (orientation given by θ), with u oriented along the major axis, roughly alongshore, positive poleward, and v oriented along the minor axis, roughly cross-shore, positive offshore. The Eulerian rms eddy speed is given by $(2\overline{EKE})^{1/2}$.

	θ_{obs}	θ_{mod}	mean_{obs}	mean_{mod}	std_{obs}	std_{mod}
SHB1 u	326°T	301°T	3.1	−2.1	7.6	9.7
SHB1 v	236°T	211°T	0.5	−0.2	1.0	0.7
SHB1 $(2\overline{EKE})^{1/2}$	-	-	7.7	9.7	-	-
M1 u	349°T	333°T	0.3	−5.1	9.9	13.5
M1 v	259°T	243°T	1.6	4.4	5.7	6.4
M1 $(2\overline{EKE})^{1/2}$	-	-	11.4	15.0	-	-
M2 u	344°T	315°T	1.3	0.6	12.9	15.8
M2 v	254°T	225°T	−2.5	3.4	9.7	8.9
M2 $(2\overline{EKE})^{1/2}$	-	-	16.2	18.1	-	-

similar, with a slightly greater range, $\sim 1-10 \times 10^{-3}$ s^{-1}. The calculation was made over depths 12–28 m, with alongshore defined by the major principal axis. Another relevant statistic for dispersal is the Eulerian rms eddy speed, which summarizes the strength of the turbulence dispersing the floats. The agreement for this statistic is much improved relative to the instantaneous velocities (Table 2). The model overestimates the eddy speed only slightly (by 10–30 percent), and the model captures the spatial structure observed between moorings, with the eddy speed increasing with water depth. In sum, the model can accurately predict many of the bulk statistics of velocity, at least in the Monterey Bay region, but it overestimates their variability by a factor of ~1.1–1.3.

3. Float processing

Approximately 1000 floats were released daily for nearly one year, from January 6, 2002 to December 31, 2002. This annual period encompasses both springtime upwelling conditions, characterized by strong offshore transport near-surface, and wintertime downwelling conditions, characterized by onshore transport near-surface. Release locations were approximately uniformly spaced within a ~3 km wide strip of coastline running along the inner shelf, excluding San Francisco Bay. The inshore edge of the strip was defined by the coastal side-wall within the numerical model, determined as the location of no normal horizontal flow, typically at a water depth of 10 or 20 m. Figure 5 shows the release locations around Point Reyes and in the northern Gulf of the Farallones. The average offshore distance of all release locations, defined as the shortest absolute distance to the coastal wall, was 1.7 km. The float-averaged water depth at release was 21 m. Particles that entered San Francisco Bay were discarded from the analysis.

Floats were tracked after release using ROMS' internal float module, which treats the floats as purely passive, Lagrangian particles. Particles are transported by the three-dimensional flow field of the model: $d\vec{x}/dt = \vec{u}(\vec{x})$, where $\vec{x}$ is the three-dimensional float position and $\vec{u}$ is the three-dimensional model velocity. The model assumes hydrostatic dynamics, and the vertical velocity is determined by the divergence of horizontal velocities. The module interpolates float positions linearly in all three spatial dimensions and integrates their positions in time using a 4th-order Milne scheme with a 4th-order Hamming corrector step. No random motion was added to the trajectories. Although new float positions were calculated within the model every baroclinic timestep (90 seconds), float positions were only recorded every 12 hours. All Lagrangian statistics are derived from these 12-hourly instantaneous "fixes."

Float displacements were calculated relative to their release locations, using Cartesian coordinates and hence a planar representation of the model grid. Displacements were then rotated into the alongshore and cross-shore directions. Alongshore (x) is aligned with the general strike of the coastline, positive toward 321°T, approximately northwestward. Cross-shore (y) is defined positive offshore, toward 231°T, approximately southwestward, with the origin at the coast. (Note, these directions differ from those used in the mooring comparison.) Velocities were calculated as the centered-in-time differences of the displacements (using

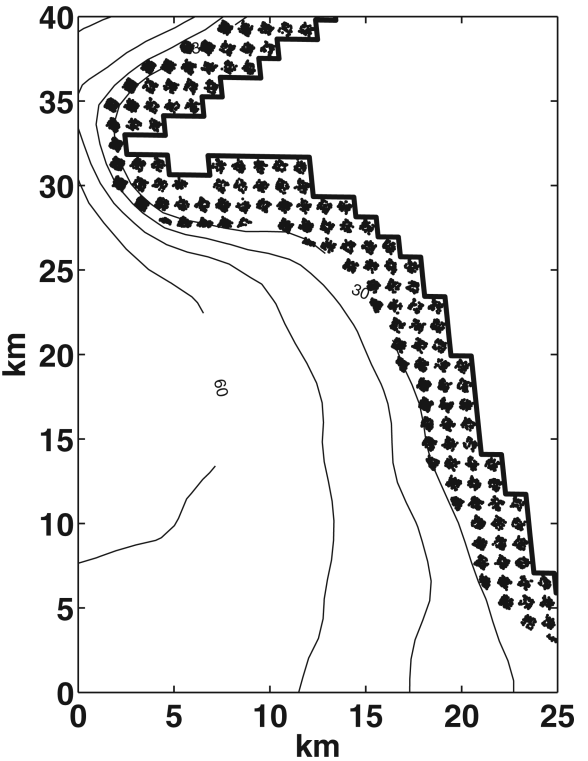

Figure 5. Close-up of float release locations around Point Reyes and in the northern Gulf of the Farallones. Heavy line is the coastal side-wall within ROMS. Fine lines are the 30, 40, 50 and 60 m isobaths. Release locations were spaced along the entire coastline (Fig. 2) in a ∼3 km wide strip running along the inner shelf, excluding San Francisco Bay.

the 12-hour fixes). All trajectory release times were then reset to $t_o = 0$, simulating an instantaneous, point-source release of particles on the inner shelf at ($x_o = 0$, $y_o = 1.7$ km, $t_o = 0$). All statistics refer to this simulated, growing cloud of floats. However, it should be remembered that the statistics refer to a time average over an entire year, and a spatial average over the coastline of central California.

Particles were released at depths of 1, 3, 6, 9, 15, 20, 25 and 30 m. Transported by the three-dimensional circulation, they quickly left their release depths and moved throughout the mixed layer and upper seasonal thermocline. They generally moved downwards with time, and their depth distribution adopted a highly skewed shape, qualitatively resembling a decaying exponential with a maximum at the surface. The float-averaged depth increased steadily from 8.6 m at release to 23 m after 16 days in the water column. Overall, float depths remained relatively shallow, with 50 percent of the floats above 16 m, 68 percent above 27 m and 95 percent above 71 m at day 16, indicating the results are representative of near-surface conditions.

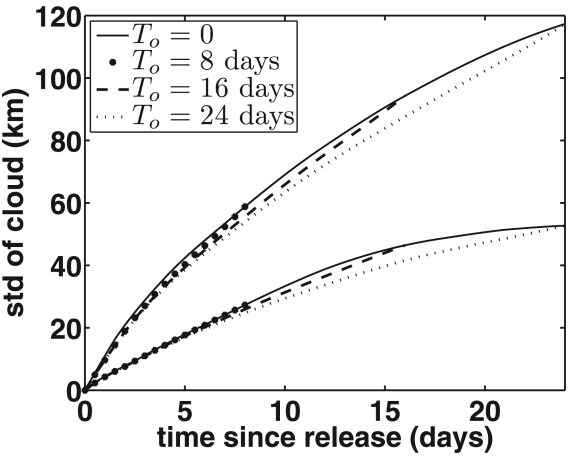

Figure 6. Float cloud standard deviation as a function of time-since-release using all available floats ($T_o = 0$) and filtered based on their presence in the domain at T_o (see Float processing). Upper curves are alongshore standard deviation, lower curves are cross-shore.

Particles were free to exit the domain through the open boundaries of the innermost grid, when they were no longer tracked by the model's float algorithm. This approach naturally creates a bias where floats released near an open boundary and the most energetic, farthest traveling floats steadily exit the domain and therefore the statistics. This particle loss is a perennial problem with Lagrangian drifter studies in limited-area domains (Baurer *et al.*, 1998; Veneziani *et al.*, 2004). To avoid any bias resulting from this loss of floats, only those remaining in the domain for a specific time period, T_o, were allowed to contribute to the statistics. However, this restriction created a more subtle bias where the most energetic floats under-contribute to the statistics at all times. The strength of the bias can be quantified in terms of the fraction of floats remaining in the domain at $t = T_o$, where t is the time-since-release. This fraction is 1.0, 0.83, 0.69 and 0.55 for T_o's of 0, 8, 16 and 24 days, respectively. (Here a T_o of 0 corresponds to allowing all floats to contribute to the statistics until they exit the domain.) We refer to this bias as "endurance" bias. The float loss can also be used as a measure of the general residence time of the domain for an inner-shelf release, with 50 percent loss at day 27.

The endurance bias did not affect the fundamental result of this study, namely the success of a simple diffusion model with linear diffusivity in describing the cross-shore float density. The measured value of the diffusivity slope, ν, where $K_y = \nu y$, was also relatively robust to changes in T_o (see Cloud growth below). However, the relevant statistics were generally sensitive to T_o, with larger values of T_o resulting in slightly slower float cloud growth (Fig. 6) and smaller mean Lagrangian velocities for any given t. For example, the alongshore standard deviation of the float cloud at $t = 8$ days was 59, 59, 56 and 54 km for T_o's of 0, 8, 17 and 24 days, respectively. The cross-shore float-averaged Lagrangian velocity, v_{rms}, when also time-averaged over days 4–8, was 9.6, 9.5, 9.2 and 9.0 cm s^{-1} for T_o's of 0, 8,

16, and 24 days, respectively. This small variation ($\leq$10 percent for the alongshore standard deviation and $\leq$7 percent for v_{rms}) suggests that the values obtained from an unlimited model domain would be very close to the values obtained here. Choosing a T_o of 16 days allowed for a reasonable compromise between the most accurate statistics and longer investigation times. Unless otherwise noted, all statistics below refer to this T_o of 16 days, using 319,834 total floats.

4. Theoretical background

The purpose of this paper is to explore the validity of a simple diffusion model in describing the cross-shore float density, when that density is treated as an Eulerian tracer. The one-dimensional diffusion equation is given by:

$$\frac{\partial \psi_y}{\partial t} = \frac{\partial}{\partial y}\left(K_y \frac{\partial \psi_y}{\partial y}\right), \tag{1}$$

where y is the cross-shore coordinate, ψ_y is the cross-shore (depth- and alongshore-integrated) float density, K_y is the cross-shore Eulerian eddy diffusivity and ψ_y is normalized such that its integral over y is unity. By adopting a model in one dimension with no advection, we implicitly treat all flow variability as turbulence, which is then parameterized by the diffusivity. This basic approach is supported by the results of Ivanov *et al.* (2008, 2009), who found no significant cross-shore advection at annual time scales for real and modeled floats launched off central California at mid-depths (275–375 m). Although this model is clearly an over-simplification, the annual averaging minimizes the importance of advection, and as we will show, the theory adequately describes many of the float statistics.

Strictly speaking, the above equation is only appropriate for a well-mixed layer of constant thickness, with zero vertical flux into or out of the layer. The observations within the numerical model do not approximate this well-mixed scenario: the vertical float distribution is highly skewed toward the surface, and there is substantial vertical shear in horizontal velocity over the relevant float depths. However, the vast majority of floats are contained within the top 30 m of the water column at all times, constituting a relatively well-defined layer. Therefore, we proceed using (1) by considering K_y as an effective depth-integrated parameter that controls the cross-shore flux of floats.

The eddy diffusivity is assumed to be zero at the coast ($y = 0$) and grow linearly with offshore distance, $K_y = \nu y$, where ν is a constant to be determined. This functional form of K_y is reasonable if diffusion is controlled by eddies whose size is limited by the presence of the coastline. This is the familiar wall-layer, mixing-length argument (Csanady, 1973, Chapter 5; Kundu, 1990, Chapter 12; Largier, 2003). Obviously, at some distance offshore this formulation will no longer apply, and the eddy size will be limited by some other process. As stated in the introduction, Davis (1985) used this form of K_y to model the position moments of near-surface floats launched over the northern California shelf and slope. And Ivanov *et al.* (2008, 2009) deduced a similar form for K_y empirically, using exit-time statistics from real floats.

Given a linear diffusivity and perfect reflection at the coast, a simple solution exists for the cross-shore float density (Huang, 1979; Ermak and Nasstrom, 2000):

$$\psi_y = \frac{1}{\nu t} \exp\left[\frac{-(y + y_o)}{\nu t}\right] I_o\left[\frac{2(y y_o)^{1/2}}{\nu t}\right], \tag{2}$$

where I_o is a modified Bessel function of the first kind of order zero, and y_o is the release location. For a release right at the coast, $y_o = 0$, Eq. (2) simplifies, becoming an exponential: $\psi_y = 1/(\nu t) \exp(-y/\nu t)$. More complex releases spread over a finite area and time period can be easily constructed from these point-source solutions by superposition (see Csanady, 1973, Chapter 1).

The position moments of ψ_y are defined as

$$\langle y^n \rangle = \int_0^\infty y^n \psi_y(y, t) dy, \quad n = 1, 2, 3 \ldots,$$

where the angle brackets represent a particle average or expectation value. Even if an exact solution for ψ_y did not exist, as it may not for alternate forms of K_y, the time evolution of the moments can be related to the diffusivity by differentiating the above equation with respect to time and substituting for $\partial \psi_y / \partial t$ from (1). Integrating the resulting equation by parts and assuming $K_y = \nu y$ and ψ_y and its derivatives approach zero faster than $y^n \to \infty$ at $y = \infty$ yields (see Davis, 1985; Hunter *et al.*, 1993; Ermak and Nasstrom, 2000):

$$\frac{\partial \langle y \rangle}{\partial t} = \nu$$

$$\frac{\partial \langle y^2 \rangle}{\partial t} = 4\nu \langle y \rangle.$$

Integrating these in time for a point-source release at $y = y_o$ gives:

$$\langle y \rangle = y_o + \nu t \tag{3}$$

$$\langle y^2 \rangle = y_o^2 + 4 y_o \nu t + 2\nu^2 t^2$$

$$\langle (y - \langle y \rangle)^2 \rangle^{1/2} = (2 y_o \nu t + \nu^2 t^2)^{1/2}, \tag{4}$$

where we have used $\langle (y - \langle y \rangle)^2 \rangle = \langle y^2 \rangle - \langle y \rangle^2$.

Eq. (3) shows the cross-shore center of mass grows linearly with time, as if the floats were transported by apparent advective velocity, ν. This well-known effect, where particles drift toward regions of high eddy energy, is referred to as the diffusion bias (Hunter *et al.*, 1993) and can be thought of as a special case of the array bias (Davis, 1991b). For releases close to the coast or at long times, (i.e., when $2y_o \ll \nu t$), the second term on the right-hand side of (4) will dominate. In these situations the cross-shore variance will grow as $\sim t^2$, and the standard deviation as $\sim t$. This linear time behavior for both the mean and standard deviation is exactly what is predicted by similarity theory for a growing cloud released at $y_o = 0$ in

a neutrally stratified turbulent wall layer (Csanady, 1973, Chapter 5). The agreement is not surprising given the choice of eddy diffusivity, which can be thought of as the product of a velocity scale and a mixing-length (see Kundu, 1990, Chapter 12). Here we have effectively assumed that the mixing length is proportional to the distance from the wall, which is one of the fundamental assumptions of similarity theory.

In practice, the cross-shore first moment, or center of mass, was calculated as

$$\langle y \rangle = y_o + P^{-1} \sum_{p=1}^{P} y'_p(t), \tag{5}$$

where y_o is the mean distance from shore at release (1.7 km), P is the total number of particles and $y'_p(t)$ is the pth particle's time-variable, cross-shore displacement relative to its release location at time t. Similarly, the cross-shore standard deviation was calculated as

$$\langle (y - \langle y \rangle)^2 \rangle^{1/2} = \left(P^{-1} \sum_{p=1}^{P} \left(y_o + y'_p(t) - \langle y \rangle \right)^2 \right)^{1/2}, \tag{6}$$

with $\langle y \rangle$ given by (5). The alongshore center of mass and standard deviation were calculated in an analogous fashion, but with $x_o = 0$, where x_o is the alongshore release location analogous to y_o.

5. Cloud growth and inferred cross-shore diffusivity

The observed alongshore and cross-shore float densities are shown in Figures 7 and 8, respectively, at various snapshots in time. The two-dimensional density (Fig. 9) is also shown at day 16. The densities were calculated with 2 km spatial bins and normalized such that their integral over all space (two- or one-dimensional) is unity. The stars indicate the location of the cloud's center of mass. From Figures 7 and 8, the float cloud can be seen to grow in the manner of an instantaneous point-source release at ($x_o = 0$, $y_o = 1.7$ km, $t_o = 0$), as intended by the processing. The large extent of the cloud indicates that the floats disperse over almost all of the model domain to some degree, but the density is orders of magnitude higher near the release location. From Figure 9, the cloud is clearly anisotropic, longer in the alongshore direction. The eastern border of the cloud extends inshore of the nominal coastline ($y = 0$) because many of the floats released near promontories, such as Point Reyes, can move into the embayments, such as the Gulf of the Farallones, causing a negative cross-shore displacement. Thus the reflective nature of the coastal boundary is spread over some finite width ($\sim$20 km) centered about $y = 0$. This is an unavoidable consequence of representing the complex coastline as a simple line, as required by the analytical solution. The fraction of floats on the landward side of the nominal boundary is small, decreasing from 0.17 to 0.07 over days 4 to 16.

The alongshore float density (Fig. 7) qualitatively resembles a slightly asymmetric Laplace distribution. Surprisingly, its peak remains at the release location ($x = 0$) at all

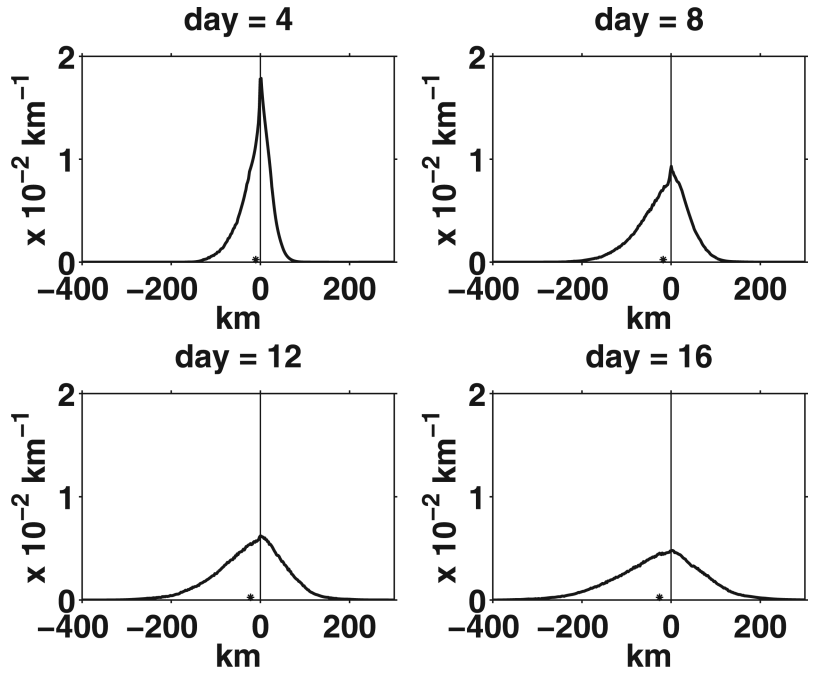

Figure 7. Alongshore particle density of a simulated cloud of floats released at $x = 0$, when averaged oven an entire year of releases and the entire length of the coastline (Fig. 2). Different panels are snapshots at progressive values of time-since-release, $t = 4$, 8, 12 and 16 days. Asterisk (dot) shows the alongshore center of mass.

times, despite the fact that the center of mass (asterisk) has moved 26 km to the south by day 16. This displacement corresponds to an average equatorward Lagrangian velocity of 1.6 cm s^{-1}. Given the strong instantaneous alongshore Eulerian velocities in the model ($\sim$25 cm s^{-1}, see Fig. 2), which are consistent with observations, this net displacement for the floats is, at first glance, surprisingly small. However, it is consistent with the relatively small alongshore Eulerian means found at the mooring sites (Table 2). The small net transport is simply a result of averaging over a year of nearshore releases, which captures both the equatorward flowing California Currnet in spring and summer and its associated poleward-flowing Inshore Countercurrent in the fall and winter (Lynn and Simpson, 1987).

The cross-shore density (Fig. 8) is negatively skewed, with most of the floats remaining relatively close to the coast. The cross-shore distribution can be put into a bathymetric context by noting that the 150 and 2000 m isobaths have an an average offshore distance of 23 and 58 km, respectively. Defining the outer edge of the continental shelf with the 150 m isobath ($\sim$23 km offshore), the center of mass can be seen to be well offshore of the shelf edge at day 16 and lies over the continental slope. Note however that there can be no exact correspondence between a given water depth and offshore distance. The presence

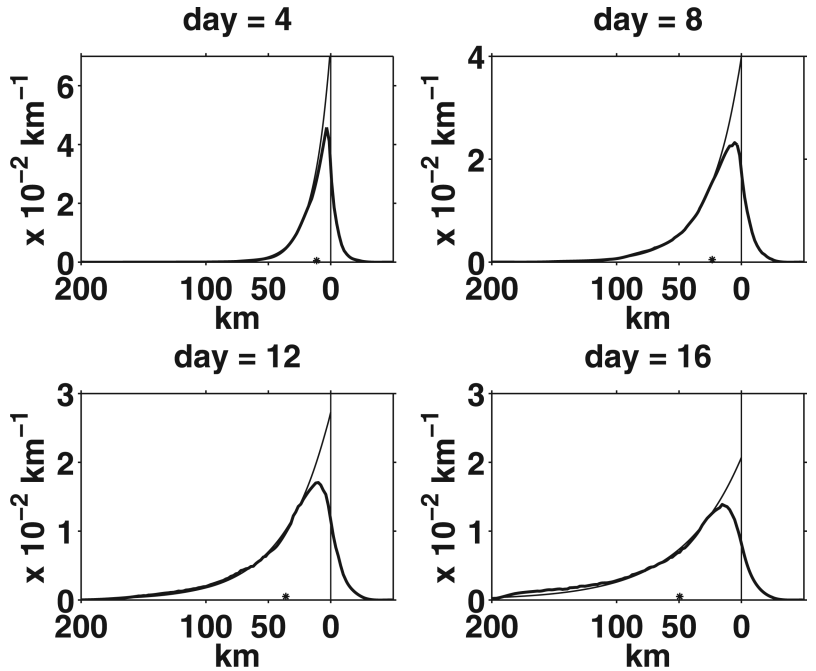

Figure 8. Cross-shore particle density of a simulated cloud of floats (heavy line) released at $y = 1.7$ km, when averaged oven an entire year of releases and the entire length of the coastline (Fig. 2). Different panels are snapshots at progressive values of time-since-release, $t = 4, 8, 12$ and 16 days. Thin solid line is the analytical solution (2) for a linear diffusivity whose offshore slope, ν, is determined from the particle moments (see Theoretical background). Asterisk (dot) shows the cross-shore center of mass.

of shallow regions, such as the Gulf of the Farallones, and steep regions, such as the Big Sur coast, introduces ambiguity into the offshore distance of any given water depth and vice versa. For example, while 6 km is the average offshore distance of the 30 m isobath, the average water depth along a curve defined as 6 km offshore of the coast is 90 m. The ambiguity can be avoided by calculating the float density as a function of water depth. Using this statistic, 68, 39 and 11 percent of the floats were found inshore of the 2000, 150 and 40 m isobaths, respectively, at day 16. Expressing this statistic as a residence time for the inner-shelf release region, defined here by the 40 m isobath, gives a 50 percent particle loss at ~2 days, and 75 percent loss at 8 days.

The instantaneous rms Lagrangian velocities (not shown) when averaged over floats, but not time, also grew without bound over days 0–16 as the cloud dispersed. Instantaneous Lagrangian velocities were calculated relative to the time-variable motion of the center of mass: $v_p(t) = d/dt(y'_p(t) - \langle y \rangle(t))$. The alongshore rms velocity increased from 11.4 to 15.6 cm s^{-1}, a roughly 35 percent increase, and the cross-shore value slightly more than doubled over the 16-day study period, ranging from 5.5 to 12.0 cm s^{-1}. This increase is

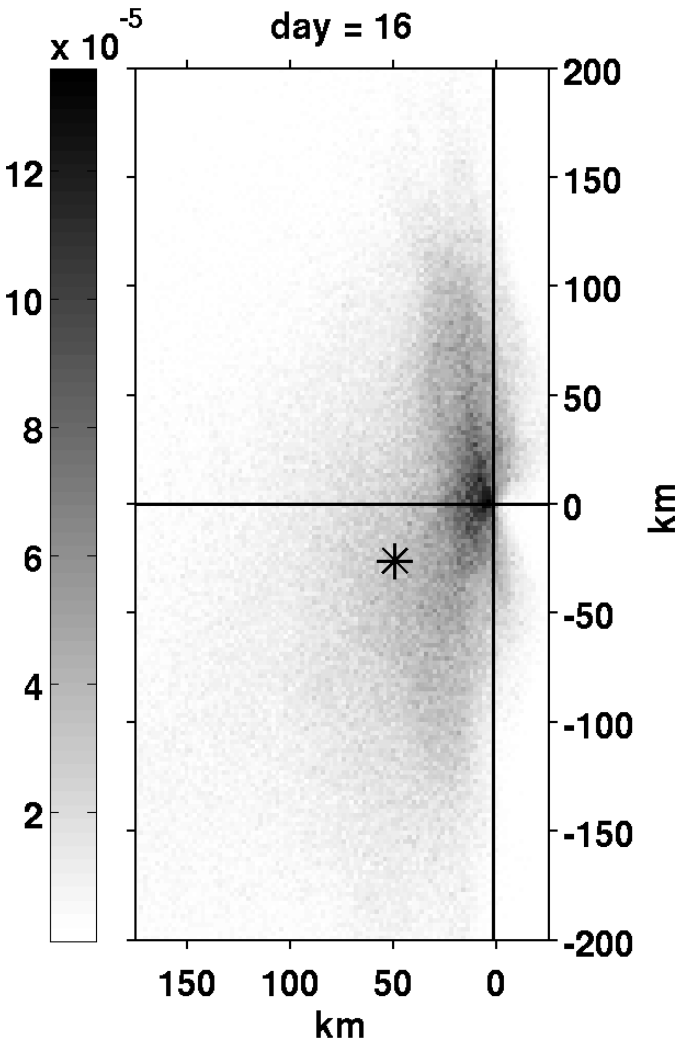

Figure 9. Two-dimensional particle density (km^{-2}) at 16 days since release for a simulated cloud of floats released near the origin at (0 km, 1.7 km), when averaged oven an entire year of releases and the entire length of the coastline (Fig. 2). Positive alongshore is oriented towards the top of the page. Black cross-hairs denote the nominal release location. Asterisk shows the cloud center of mass.

simply a consequence of the lack of spatial homogeneity, clearly seen in the mean and rms Eulerian velocity field (Fig. 3). As the floats diffuse away from the inner shelf, especially the relatively quiescent environment of the Gulf of the Farallones, their statistics evolve. Time- and float averaged values for the rms Lagrangian velocities are $(\overline{u}_{rms}, \overline{v}_{rms}) = (13.9, 9.6)$ cm s^{-1}, where the overbar represents a time average.

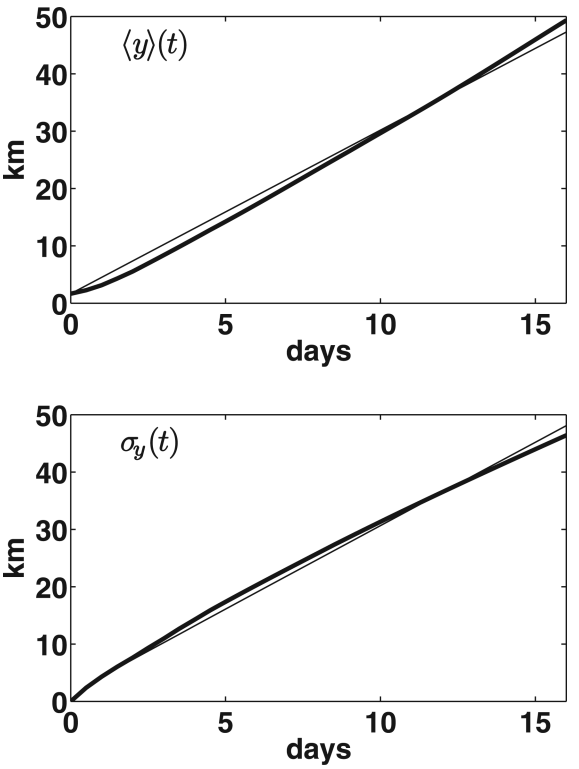

Figure 10. Top panel: time-evolution of the cloud's cross-shore center of mass as observed from (5), heavy line, overlain with a least-squares best fit to the prediction of a linear diffusivity (3), light line. Bottom panel: time evolution of the cloud's cross-shore standard deviation as observed from (6), heavy line, overlain with a least-squares best fit to the prediction of a linear diffusivity (4), light line.

The observed time evolution of the cloud's cross-shore center of mass, $\langle y \rangle$, as determined from (5) is shown as the heavy line in the top panel of Figure 10. The growth is nearly linear, as predicted by the simple diffusion model with linear diffusivity (3). A least-squares best fit of the observed $\langle y \rangle$ to the right-hand side of (3) is shown as the thin line in the top panel. The fit yields a value for ν of 3.3 cm s^{-1}. Similarly, the observed cross-shore standard deviation, determined from (6), is shown as the heavy line in the bottom panel of Figure 10. An analogous fit of the standard deviation to the right-hand side of (4) is shown as the thin line in the bottom panel and gives $\nu = 3.4$ cm s^{-1}. (For both fits, a constant y_o of 1.7 km was used.) The two semi-independent estimates of ν agree surprisingly well. As a diffusion model alone can explain the time evolution of the cloud moments, there appears to have been no net effective cross-shore advection for the floats when averaged over an entire year. The offshore movement of the floats and the cloud center of mass is due entirely to an array bias (see Theoretical background above).

Davis (1985) performed a similar analysis in the CODE region (north of Point Reyes) using real surface drifters from May and July deployments. Also assuming a linear Eulerian diffusivity, he determined a value of $\nu = 0.8$ cm s^{-1}. However, his model incorporated substantial advection, determined from large offshore Eulerian velocities ($\sim$20 cm s^{-1}) not present in our annually averaged model output. When using direct measurements of the Lagrangian diffusivity from drifter trajectories, however, he found a similar linear offshore increase in the diffusivity with slope 3 cm s^{-1}, very close to the value of ν found here.

Given a ν of 3.4 cm s^{-1} determined from the cross-shore moments, we compare the cross-shore float density to the analytical solution (2), shown as the thin line in Figure 8. The analytical solution does an excellent job of predicting the observations over most of the domain. There is substantial disagreement over the mid- and inner shelf, but this likely results from the approximation of the complex coastline as a straight line, as noted above. In addition, there may be some small net advective velocity over the shelf that also shifts the peak density offshore.

Shortening the total investigation time, and hence T_o, to 8 days influenced ν only slightly, yielding values of 3.2 and 3.7 cm s^{-1} from fits to (3) and (4), respectively. Extending the investigation time to 24 days resulted in noticeably poorer agreement with the analytical solution after day 18 (not shown) regardless of the choice of ν. It also resulted in a poorer fit to (4). However, the center of mass was $\geq$50 km offshore by day 18, as were 40 percent of the floats. Thus the fundamental assumption of a linear diffusivity is likely breaking down at these times, with a large fraction of the floats no longer directly influenced by the coast. For $T_o = 24$ days, fitted values of ν were 3.0 and 2.8 cm s^{-1} from (3) and (4), respectively. The variation in ν found here results from altering both the investigation time and the endurance bias. The effect of the endurance bias on ν can be isolated by restricting the fits to days 4–8 and varying T_o. This yielded a variation in ν of $\leq$15 percent, demonstrating that ν is relatively insensitive to the endurance bias, as stated previously (see Float processing).

6. Cross-shore mixing length

Given the success of the linear diffusivity model, $K_y = \nu y$, at predicting the time evolution of the cross-shore moments and float density, we now explore its implications. The eddy diffusivity is traditionally viewed as the product of a mixing length, l, and a turbulent velocity scale, u_*: $K = u_* l$. At face value, the above two relations imply a mixing length equal to the distance from the coast, $l = y$, with corresponding turbulent velocity scale, $u_* = \nu$. However, the time- and float-averaged cross-shore rms Lagrangian velocity, $\overline{v}_{rms}$, was found to be $\sim 3\nu$ (9.6 cm s^{-1} vs. 3.4 cm s^{-1}), indicating a different interpretation of the mixing length is needed.

Another natural choice for the mixing length is the local internal Rossby radius of deformation. There is growing observational evidence of a strong relationship between the first

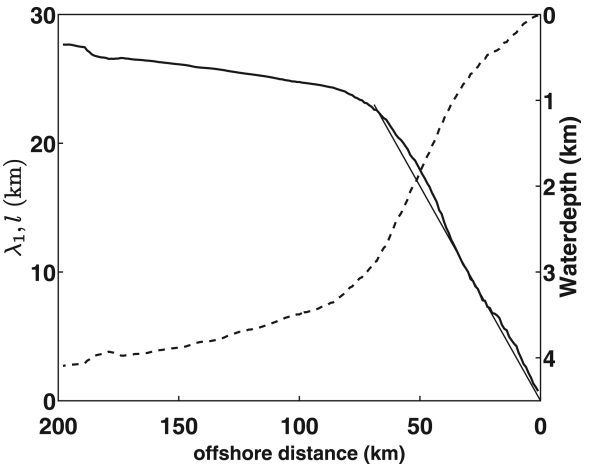

Figure 11. First mode internal Rossby radius as a function of offshore distance (heavy solid line), scaled on left-hand y-axis. Heavy dashed line is water depth, averaged analogously to the Rossy radius, scaled on right-hand y-axis. Thin solid line is the implied mixing length, l, determined from the cross-shore cloud moments and the rms Lagrangian velocity (see Cross-shore mixing length).

mode internal Rossby radius, λ_1, and the Lagrangian integral length scale (Eden, 2007; Zhurbas and Oh, 2003). These studies occurred at midlatitudes in deep water, where the implication is that quasi-geostrophic mesoscale eddies are controlling the lateral mixing. An analogous relationship may exist over the continental shelf and slope, where λ_1 may determine the cross-shore mixing length. If λ_1 varies primarily with offshore distance, and $\overline{v}_{rms}$ is taken as the turbulent velocity scale, a traditional scaling for the diffusivity implies: $K_y = \overline{v}_{rms}\lambda_1(y)$. Given $K_y = \nu y$, the preceding equation suggests $\nu \sim \overline{v}_{rms} d\lambda_1/dy$.

The first mode of the local Rossby radius, λ_1, was calculated in the manner of Chelton *et al.* (1998) using the time-mean density stratification averaged over the annual study period. They give $\lambda_1 = \int_{-H}^{0} N(z)/(|f|\pi)dz$, where H is the water depth, N is the buoyancy frequency and f is the Coriolis parameter. The calculation was performed for each horizontal model gridpoint. The offshore distance of each gridpoint, defined as the shortest distance from each gridpoint to any point on the non-linearized coastline, was also determined. The values of λ_1 were then averaged within bins of equal offshore distance, allowing for a smooth plot of λ_1 versus offshore distance, y. These values of λ_1 are shown as the heavy solid line in Figure 11. (An alternate method of spatially averaging λ_1, averaging over bins of equal water depth and then calculating the offshore distance of those bins, yielded similar, but noisier, results. Thus the ambiguity between offshore distance and water depth noted above in the Cloud growth section had only a minor effect on λ_1.) The variation in λ_1 is surprisingly linear over the shelf and slope, with a break in the slope of the curve near $y = 70$ km, $H = 3000$ m. A linear regression over the shoreward region, $0 < y < 70$ km, yields $\lambda_1 = 0.18 + 0.34y$, in km. Ignoring the small intercept gives $\nu \sim (9.6)(0.34) \sim 3.3\,\mathrm{cm\,s^{-1}}$,

in good agreement with the values of ν determined as best fits to the particle moments. As a more visual comparison, we have plotted the implied mixing length, $l = \nu y/\overline{v}_{rms}$, as the thin line in Figure 11, using a ν of 3.4 cm s^{-1}. The agreement with λ_1 is striking. Although this near-exact agreement may be fortuitous, it strongly suggests the first mode internal Rossby radius plays an important role in the cross-shore mixing.

7. Discussion

a. Alternate diffusivity models

It was mentioned in the Cloud growth section above that the instantaneous rms Lagrangian cross-shore velocity increased by slightly more than a factor of two as the cloud grew over the 16-day study period. Strictly speaking, this increase is inconsistent with the idea of a single, dominant turbulent velocity scale contributing to the Eulerian diffusivity. The time-increase in $\overline{v}_{rms}$ results from the cloud dispersing further offshore, where the Eulerian Eddy Kinetic Energy is generally larger (Fig. 3). The cross-shore rms Eulerian velocity, v_e, also grew with distance from the coast (not shown). Here, v_e was calculated at a depth of 20 m and spatially averaged in bins of equal offshore distance, analogous to the treatment of the Rossby radius, to convert it into a univariate function of y. Values of v_e increased from 5.1 to 11 cm s^{-1} roughly linearly over a segment near the coast ($y = 0 - 45$ km) and continued to increase monotonically up to a maximum of 17 cm s^{-1} at 125 km offshore. Given the behavior of v_e, one could also arrive at a linear diffusivity by arguing the turbulent velocity scale was a linear function of offshore distance while the mixing length was roughly constant. In other words, $K_y = v_e(y)l_o$, where l_o is a constant mixing length. To explore this alternate model, we estimate l_o as the product of a turbulent velocity scale ($\overline{v}_{rms}$) and a time scale over which this velocity changes appreciably. Estimating this time-scale as the integral of the normalized autocorrelation function (Bendat and Piersol, 2000) of $v_{rms}(t)$ out to its first zero crossing (not shown), yields a turbulent time scale of ~1 day and l_o ~10 km. Performing a regression for the Eulerian rms cross-shore velocity versus offshore distance and assuming $\nu \sim l_o dv_e/dy$, then yields $\nu \sim 1$ cm s^{-1}, which is substantially lower the values of ν determined from the moments. The non-zero value of v_e at the coast also prevents K_y from going to zero there, which is inconsistent with similarity theory. Thus a K_y determined by a variable mixing length set by λ_1 is more consistent with the observations than a K_y set by a variable velocity scale.

Taking the idea of a spatially variable diffusivity still further, the linear cross-shore structure of both $v_e \sim y$ and $\lambda_1 \sim y$ imply $K_y \sim Ay^2$, where A is a constant. However, using a quadratic shape for K_y in a numerical solution to the one-dimensional diffusion equation did not improve the agreement with the observed float density, relative to the linear K_y case, regardless of the choice of A. The mixing length theory is semi-empirical, and in general the turbulence may not have a dominant velocity or length scale. However, these simple mixing arguments can be used to adequately describe the cross-shore moments, the float density over the outer shelf and slope, and to link offshore diffusion to a fundamental parameter, the first mode internal Rossby radius. These results are encouraging in that

traditional conceptualizations of dispersion, such as employing a linear diffusivity near a side-wall boundary, can be extended to a realistic simulation of the coastal ocean, and potentially the real ocean. Although there are many differences between the a traditional turbulent wall layer and the ocean's horizontal circulation over the continental shelf and slope, it appears the influence of the internal Rossby radius on the cross-shore mixing allows the use of the familiar theories.

b. Tidal dispersion

Despite the fact that the subtidal circulation contributes most of the total current variance in the central California coastal ocean (Kaplan *et al.*, 2005), tidal-band currents can be important, with instantaneous values reaching up to $\sim$30 cm s^{-1} at specific locations (Rosenfeld *et al.*, 2009). The numerical model was not forced with tidal motions or a seabreeze, and is thus neglecting a relatively small but potentially substantial source of dispersion. The relative importance of tidal-band motions can be quantified by estimating the tidal-band diffusivity, which will contribute linearly to the total diffusivity if tidal-band and subtidal motions are uncorrelated. The tidal diffusivity can be scaled as $K_t \sim u_t^2 T_t$, where u_t is a representative tidal velocity ($\sim$10 cm s^{-1}, Kaplan *et al.*, 2005) and T_t is a tidal time scale ($\sim$4 hours, the decorrelation time-scale at first zero-crossing for a diurnal oscillation). These values give $K_t \sim$150 m^2 s^{-1}. As alongshore diffusivities over the northern California shelf are $\sim$3500 m^2 s^{-1} (Davis, 1985), tidal-band motions should be negligible relative to the overall alongshore dispersion. The cross-shore diffusivity, however, grows with distance from shore (see above and Davis, 1985). Therefore there will be some near-coast region where the tidal-band and mesoscale dispersion are comparable ($y \lesssim$ 10 km using the value of ν found here). Understanding dispersion at all time scales in this region of the the central California coastal ocean is a fertile area for future research.

8. Summary

A high-resolution numerical simulation of the central California coastal ocean was used to study cross-shore particle dispersion over the continental shelf and slope. Particles were released daily along the inner shelf for one model year and tracked for 16 days, yielding over 300,000 individual near-surface trajectories. The particles were treated statistically as an instantaneous point-source release, dispersing away from the inner shelf as an Eulerian tracer cloud. The cross-shore particle statistics were well-described by a simple Eulerian diffusion model employing a linear diffusivity, $K_y = \nu y$, where y is the cross-shore coordinate and ν a constant. The theoretical model adequately described the time-evolution of the particle-averaged mean and standard deviation of position. Fitting the model to the observations yielded a value of ν of $\sim$3–4 cm s^{-1}. In addition, an analytical solution of the model accurately predicted the particle density over the outer shelf and slope. The linear diffusivity implied a linear cross-shore mixing length, which was found to be equal to the local first mode Rossby radius of deformation.

Acknowledgments. The authors thank the Monterey Bay Research Aquarium Institute (MBARI) for its generous contribution of mooring data and two anonymous reviewers for their helpful suggestions. This is contribution number 326 from PISCO, the Partnership for Interdisciplinary Studies of Coastal Oceans, a long-term ecological consortium funded primarily by the Gordon and Betty Moore Foundation and the David and Lucile Packard Foundation.

REFERENCES

Bauer, S., M. S. Swenson, A. Griffa, A. J. Mariano, and K. Owens. 1998. Eddy-mean flow decomposition and eddy-diffusivity estimates in the tropical Pacific Ocean 1. Methodology. J. Geophys. Res., *103*, 30,855–30,871.

Bendat, J. S. and A. G. Piersol. 2000. Random Data, John Wiley and Sons, NY.

Boning, C. W. and M. D. Cox. 1988. Particle dispersion and mixing of conservative properties in an eddy-resolving model. J. Phys. Oceanogr., *18*, 320–338.

Chelton, D. B., R. A. deSzoeke, and M. G. Schlax. 1998. Geographical variability of the first baroclinic Rossby radius of deformation. J. Phys. Oceanogr., *28*, 433–460.

Csanady, G. T. 1973. Turbulent Diffusion in the Environment, D. Reidel Publishing, Boston.

Davis, R. E. 1985. Drifter observations of coastal surface currents during CODE: The statistical and dynamical views. J. Geophys. Res., *90*(C3), 4,756–4,772.

—— 1991a. Lagrangian ocean studies. Annu. Rev. Fluid Mech., *23*, 43–64.

—— 1991b. Observing the general circulation with floats. Deep-Sea Res., *38*(Suppl. 1), S531–S571.

Drake, P. T., M. A. McManus, and C. D. Storlazzi. 2005. Local wind forcing of the Monterey Bay area inner shelf. Cont. Shelf Res., *25*, 397–417.

Eden, C. 2007. Eddy length scales in the North Atlantic Ocean. J. Geophys. Res., *112*, doi: 10.1029/2006JC003901.

Ermak, D. L. and J. S. Nasstrom. 2000. A Lagrangian stochastic diffusion method for inhomogeneous turbulence. Atmos. Environ., *34*, 1,059–1,068.

Heimbach, P. 2008. The MITgcm/ECCO adjoint modeling infrastructure. CLIVAR Exchanges, *13(1)*, 13–17.

Heimbach, P., R. M. Ponte, C. Evangelinos, G. Forget, M. Mazloff, D. Menemenlis, S. Vinogradov, and C. Wunsch. 2006. Combining altimetric and all other data with a general circulation model, *in* Proceedings of the 15 Years of Progress in Radar Altimetry Symposium, Venice, 13–18 March 2006, Vol. SP-614, ESA Publications Division, 2200 AG Noordwijk, The Netherlands.

Hodur, R. M. 1997. The Naval Research Laboratory's Coupled Ocean/Atmosphere Mesoscale Prediction System (COAMPS). Mon. Weather Rev., *135*, 1,414–1,430.

Hodur, R. M., J. Pullen, J. Cummings, X. Hong, J. D. Doyle, P. Martin, and M. A. Rennick. 2002. The Coupled Ocean/Atmosphere Mesoscale Prediction System (COAMPS). Oceanography, 15, 88–98.

Huang, C. H. 1979. A theory of dispersion in turbulent shear flow. Atmospheric Environment, *13*, 453–463.

Hunter, J. R., P. D. Craig, and H. E. Phillips. 1993. On the use of random walk models with spatially variable diffusivity. J. Comput. Phys., *106*, 366–376.

Ivanov, L. M., C. A. Collins, P. Marchesiello, and T. M. Margolina. 2009. On model validation for meso/submesoscale currents: Metrics and application to ROMS off central California. Ocean Model., *28*, 209–225.

Ivanov, L. M., C. A. Collins, T. M. Margolina, L. I. Piterbarg, and V. N. Eremeev. 2008. On westward transport processes off central California revealed by RAFOS floats. Geophys. Res. Lett., *35*, doi: 10.1029/2008GL034689.

Kaplan, D. M., J. Largier, and L. W. Botsford. 2005. HF radar observations of the surface circulation off Bodega Bay (northern California, USA). J. Geophys. Res., *110*, doi: 10.1029/2005JC002959.

Kosro, P. M., A. Huyer, S. R. Ramp, R. L. Smith, F. P. Chavez, T. J. Cowles, M. R. Abbott, P. T. Strub, R. T. Barber, P. Jessen, and L. F. Small. 1991. The structure of the transition zone between coastal waters and the open ocean off northern California, winter and spring, 1987. J. Geophys. Res., *96*(C8), 14,707–14,730.

Kundu, P. K. 1976. Ekman veering observed near the ocean bottom. J. Phys. Oceanogr., *6*, 238–242.

—— 1990. Fluid Mechanics, Academic Press, San Diego.

Large, W. G., J. C. McWilliams, and S. C. Doney. 1994. Oceanic vertical mixing: a review and a model with a non-local K-profile boundary layer parameterization. Rev. Geophys., *32*, 363–403.

Largier, J. L. 2003. Considerations in estimating larval dispersal distances from oceanographic data. Ecol. Appl., *13*(Suppl.), S71–S89.

Lumpkin, R., A.-M. Treguier, and K. Speer. 2002. Lagrangian eddy scales in the North Atlantic Ocean. J. Phys. Oceanogr., *32*, 2,425–2,440.

Lynn, R. J. and J. J. Simpson. 1987. The California Current System: The seasonal variability of its physical characteristics. J. Geophys. Res., *92*(C12), 12,947–12,966.

Okubu, A. 1971. Oceanic diffusion diagrams. Deep-Sea Res., *18*, 789–802.

Rosenfeld, L. K., F. B. Schwing, N. Garfield, and D. E. Tracy. 1994. Bifurcated flow from an upwelling center: a cold water source for Monterey Bay. Cont. Shelf Res., *14*, 931–964.

Rosenfeld, L., I. Shulman, M. Cook, J. Paduan, and L. Shulman. 2009. Methodology for a regional tidal model evaluation, with application to central California. Deep-Sea Res. II, *56*, 199–218.

Roughan, M., N. Garfield, J. Largier, E. Dever, C. Dorman, D. Peterson, and J. Dorman. 2006. Transport and retention in an upwelling region: The role of across-shelf structure. Deep-Sea Res. II, *53*, 2,931–2,955.

Shchepetkin, A. F. and J. C. McWilliams. 2005. The regional oceanic modeling system (ROMS): a split-explicit, free-surface, topography-following-coordinate oceanic model. Ocean Model., *9*, 347–404.

Strub, P. T., P. M. Kosro, and A. Huyer. 1991. The nature of cold filaments in the California Current System. J. Geophys. Res., *96*(C8), 14,743–14,768.

Swenson, M. S. and P. P. Niiler. 1996. Statistical analysis of the surface circulation of the California Current. J. Geophys. Res., *101*(C10), 22,631–22,645.

Taylor, G. I. 1921. Diffusion by continuous movements. P. Lond. Math. Soc., *20*, 196–212.

Veneziani, M., A. Griffa, A. M. Reynolds, and A. J. Mariano. 2004. Oceanic turbulence and stochastic models from subsurface Lagrangian data for the Northwest Atlantic Ocean. J. Phys. Oceanogr., *34*, 1,884–1,906.

Veneziani, M., C. A. Edwards, J. D. Doyle, and D. Foley. 2009. A Central California coastal ocean modeling study. Part I: The forward model and the influence of realistic versus climatological forcing. J. Geophys. Res., *114*, doi: 10.1029/2008JC004774.

Winant, C. D., R. C. Beardsley, and R. E. Davis. 1987. Moored wind, temperature, and current observations made during coastal ocean dynamics experiments 1 and 2 over the northern California continental shelf and upper slope. J. Geophys. Res., *92*(C2), 1,269–1,604.

Wunsch, C, R. M. Ponte, and P. Heimbach. 2007. Decadal trends in sea level patterns: 1993–2004. J. Climate, *20*, 5,889–5,911.

Zhurbas, V. and I. S. Oh. 2003. Lateral diffixsivity and Lagrangian scales in the Pacific Ocean as derived from drifter data. J. Geophys. Res., *108*(C5), doi: 10.1029/2002JC001596.

Received: *26 February, 2009*; revised: *28 August, 2009*.